The rheological characterization of linear viscoelasticity for ink jet fluids using piezo axial vibrator and torsion resonator rheometers

D. C. Vadillo[a)]

Department of Chemical Engineering and Biotechnology, University of Cambridge, Cambridge CB2 3RA, United Kingdom

T. R. Tuladhar

Xaar Technology, Cambridge CB4 0XR, United Kingdom

A. C. Mulji and M. R. Mackley

Department of Chemical Engineering and Biotechnology, University of Cambridge, Cambridge CB2 3RA, United Kingdom

(Received 4 August 2009; final revision received 16 April 2010; published 8 June 2010)

Synopsis

This paper is concerned with the experimental ability to measure viscoelasticity of low viscosity ink jet fluids and demonstrates the capability of both a piezo axial vibrator and torsion resonator rheometer to capture high frequency rheological data for both model and commercial ink jet fluids. Results are presented for polymer and particle laden suspensions together with a commercial ink. The data demonstrate that high frequency linear viscoelastic rheology can be captured using both rheometers and that both the presence of polymer and particles can induce viscoelasticity within the fluid. It is believed that the physical origin of viscoelastic effects produced by the presence of polymer or particles is different, and this results in a different high frequency limiting slope for the G′ data. © *2010 The Society of Rheology.* [DOI: 10.1122/1.3439696]

I. INTRODUCTION

The linear viscoelastic (LVE) response of a fluid is generally at the core of many processing effects for the fluid. In the past, most LVE measurements of these fluids have been carried out using oscillatory rheometers that have relied on mechanical motor driven oscillation. For polymer melts, this has generally worked well, as the engineering relevant relaxation modes of the polymer were generally within the angular frequency regime of most mechanical spectrometers; namely, 0.01–100 rad/s (http://www.tainstruments.com/, http://www.malvern.com). The low frequency limit usually relates to low stress signal to noise levels and the higher limit to motor oscillation limitations and/or inertia effects [Macosko (1994); Whorlow (1992)]. Sometimes, in relation to modeling viscoelastic behavior, a wider range of frequencies is required [Auhl *et al.*

[a)]Author to whom correspondence should be addressed; electronic mail: dv244@cam.ac.uk

(2008); Walters (2007)] and often this could be established using what has now become standard time temperature superposition (TTS) data shifting [see, for example, Ferry (1980); Auhl *et al.* (2008)].

Low viscosity fluids can also exhibit viscoelasticity; however, the relaxation modes for these materials are usually very much shorter and in the time domain of milliseconds or below. In general, TTS cannot be used to access these short mode relaxation times and different rheometers need to be used. A series of high frequency torsional resonator rheometers has been built and these have been successful in obtaining data at specific resonant frequencies [Theobald *et al.* (1994); Bergenholtz *et al.* (1998); Kirschenmann and Pechhold (2002); Fritz *et al.* (2003)]. More recently, piezodevices have been developed to cover a range of frequencies [Groβ *et al.* (2002); Crassous *et al.* (2005)] and laser optic systems have also been used to capture time modulated optical scattering events [Willenbacher *et al.* (2007), http://www.lsinstruments.ch/].

Ink jet droplet formation is a very delicate process and the ink jet fluids fall into the class of potentially weakly viscoelastic, low viscosity fluids. Fromm (1984) demonstrated, using dimensional analysis, that the drop formation mechanism is controlled by the Reynolds number (ratio of the inertia to viscous force, $\mathrm{Re}=\rho \mathrm{D}_0\mathrm{U}/\eta_0$) and the Weber number (ratio of the inertia to surface tension force, $\mathrm{We}=\rho \mathrm{D}_0\mathrm{U}^2/\sigma$), where ρ is the fluid density, D_0 is the nozzle diameter, U is the fluid velocity, η_0 is the zero shear rate viscosity of the fluid, and σ is the fluid surface tension. The competition between the fluid viscosity and fluid surface tension, quantifiable by the Ohnesorge number ($\mathrm{Oh}=\eta_0/\sqrt{\rho \mathrm{D}_0\sigma}$), also plays an important role. It has been experimentally demonstrated that a printable fluid should obey $1<\mathrm{Z}<10$, where $\mathrm{Z}=1/\mathrm{Oh}$ [Fromm (1984); Dong *et al.* (2006); Jang *et al.* (2009)]. The lowest value of Z is governed by the dissipation of the pressure wave by the viscosity of the fluid, whereas the higher limit is determined by the fact that the fluid forms satellite droplets instead of a unique droplet. Such studies did not take into account the viscoelastic behavior of ink jet fluids which also influences the process and comes from the polymer dispersant and solid particles that exist in ink jet inks. Ink jet fluids are usually characterized by a zero shear rate viscosity of order 20 mPa s or less at their jetting temperature and previous experiments report very little shear thinning behavior even at high shear rates [Tuladhar and Mackley (2008)]. The jetting of fluids containing polymer solution has been studied experimentally and results reported a decrease of the jetting velocity and an increase of the filament length outside the printhead with the addition of polymer [Basilevsky *et al.* (2005); Xu *et al.* (2007)]. An increased applied wave form can often compensate for the increase in viscoelasticity due to polymer addition. Hoath *et al.* (2009) performed the first experimental investigation, linking the jetting of a viscoelastic fluid and the high frequency LVE rheology of the fluid. These authors showed that there was a direct link between the ratio G'/G^* (where G' is the elastic modulus of the fluid and G^* is the complex modulus of the fluid) with jetting behavior and in general a value of G'/G^* at 5 kHz of 5% gave optimal performance. Below this value, satellite formation was a problem and above this value, thread formation introduced jetting difficulties. Vadillo *et al.* (2010) subsequently correlated the fluid jettability and the nonlinear fluid rheology using filament stretching experiments combined with high speed imaging. They showed that the addition of a small amount of polymer modified the filament breakup profile just prior the pinch-off by creating a small tail without increasing significantly the extensional viscosity. These observations have subsequently been correlated with drop formation mechanism and it has been shown that an optimized concentration of added polymer can reduce or prevent the satellite formation [Vadillo *et al.* (2010)].

The quantification of the ink jet fluid's linear viscoelasticity is therefore desirable. In

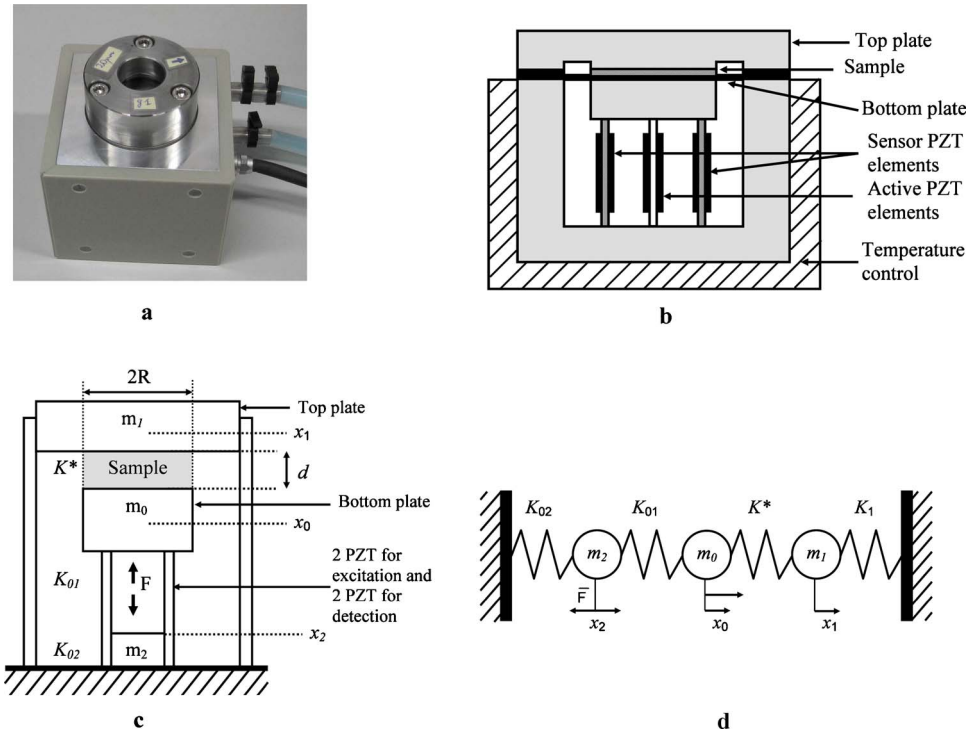

FIG. 1. (a) Photograph of PAV, (b) schematic of PAV, (c) geometric analog of PAV, and (d) mechanical analog of PAV. (b)–(d) have been reproduced from Kirschenmann (2003) and Crassous *et al.* (2005).

this paper, high frequency LVE data for ink jet fluids are characterized using two established rheometers: the piezoaxial vibrator (PAV) [Crassous *et al.* (2005)] and the torsion resonator (TR) [Fritz *et al.* (2003)] that can access the relevant time domain for ink jet fluids. Model polymer solutions, model inks, and industrial inks are considered and this paper also demonstrates that the LVE response of different model fluids can be different depending on whether the elasticity originates from polymer or particle behavior.

II. EXPERIMENTAL APPARATUS AND FLUIDS TESTED

A. The PAV

The PAV is a dynamic squeeze flow rheometer that operates at frequencies between 1 and 10 000 Hz (below its resonance frequency) that has been used to characterize the linear viscoelasticity of soft matter fluids such as blood [Groß *et al.* (2002)] and low viscosity polymeric solutions [Crassous *et al.* (2005); Hoath *et al.* (2009)]. Figure 1(a) shows a photograph of the PAV unit with a glass top plate and a schematic of this apparatus is presented in Fig. 1(b). The PAV is built around four thin walled stainless steel rectangular tubes on which eight piezoelectric (PZT) elements are glued (two on each side of each wall: inside and outside). Four active PZTs are attached to two opposite walls of the tube in order to exert vibrations while additional passive PZTs are fixed to the remaining sides in order pick up the response signal. Direct coupling of excitation and detection is avoided by four partial lengthwise cuts of the tube between active and sensor PZT elements. The rectangular tubes are glued to a rigid base and surrounded by a hollow cylinder. The top section of the tube and cylinder are tightly covered by a thick stainless

plate (which serves as the bottom plate of the sample) with a circular radius R. Using a stainless steel microfoil distance ring, the PAV can be hermetically closed with a thick stainless steel, glass, or sapphire top plate, leaving a circular gap of depth d (between 5 and 200 μm) to be filled by squeeze flow of a test fluid. In the present work, all experiments have been performed using the stainless steel top plate. The lower part of the device is surrounded by a double walled cylinder allowing the circulation of fluid for temperature control [Figs. 1(a) and 1(b)].

The PAV mechanical equivalent diagram is shown in Figs. 1(c) and 1(d). Mechanically, the system is modeled as four elastic elements of stiffness K_i linked to three masses m_i [Fig. 1(d)] [Kirschenmann (2003); Crassous *et al.* (2005)]. K_{01} is the spring constant of the tube length stuck with PZT elements, $K_{02}(\gg K_{01})$ is the spring constant of the passive part of the tube, and K_1 is the lumped spring constant of the frame including that of top plate. The rigidity K_0 of the cylinder $[K_0 = K_{01} \cdot K_{02}/(K_{01} + K_{02})]$ must at least be 1×10^8 N m^{-1} to assure a high resonance frequency for the head of the probe and the cylinder. Therefore, the sample rigidity, K^*, should be lower than 10^9 N m^{-1}. K^* can be derived from the apparatus response by experimentally measuring the stiffness response of the system, with and without the sample [Crassous *et al.* (2005)]. The PAV is operated by a lock-in-amplifier (SR 850, Stanford Research Systems) with an exciting voltage of 5 V which (in our version of the driving piezo) is proportional to an axial force F and results in a maximum displacement of around 10 nm of the lower plate, which corresponds to a maximum strain between 0.01% and 0.2%. An unloaded test enables the measurement of the dynamic displacement x_0 of the lower plate at a given frequency leading to the compliance x_0/F. The sample is then loaded and the same measurement is repeated at the same frequencies leading to the modulated compliance x/F. The complex ratio x/x_0 leads to K^* which can be calculated from solving a set of the equations of motion for each of the masses shown in Fig. 1(d). K^* can then be related to the complex modulus G^* of the test fluid using standard squeeze flow LVE analysis as shown in

$$K^* = \frac{\frac{3\pi}{2} R \left(\frac{R}{d}\right)^3 G^*}{1 + \frac{\rho \omega^2 d^2}{10 G^*} + \cdots}, \tag{1}$$

where ρ is the sample density, ω is the angular frequency of oscillation, and G^* is the complex modulus of the test fluid with $G^* = G' + iG''$, where G' is the storage modulus and G'' is the loss modulus. Inertia is taken into account in the denominator of the equation which may become important at high frequency. For the above equation, the fluid is assumed to be incompressible; however, this condition can be relaxed if required. The dynamic compressibility κ^* of the fluid can introduce an artificial elasticity, in particular, at high frequency for low viscosity fluid and must subsequently be corrected. For squeeze flow, in the limit of small amplitudes, Kirschenmann (2003) obtained

$$K^* = \frac{2}{3\pi} \frac{d^3}{R^4} \left(\frac{1}{G^*} + \frac{3}{2} \left(\frac{R}{d}\right)^2 \kappa^* \right). \tag{2}$$

The strong dependence of Eqs. (1) and (2) on the ratio R/d indicates that the repetition of the experiments for different gap depths d (R has a fixed value of 10 mm here) enables the fluid compressibility problem to be addressed leading to accurate measurements over the frequency range of the PAV with reliable G^* as low as 0.1 Pa. In the present work, gap depths of 5, 13, 38, 61, and 113 μm have been used, allowing fluid samples to be

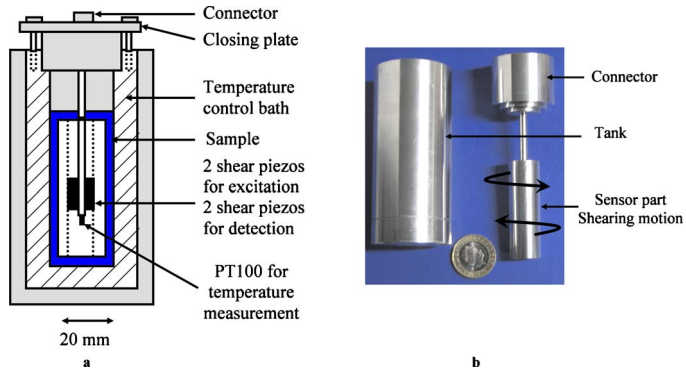

FIG. 2. (a) Schematic diagram of TR and (b) photograph of TR.

adequately characterized. More details of the mathematical calculation are not presented here but can be found in Kirschenmann (2003).

B. TR

The TR is a dynamic torsion flow rheometer used to characterize linear viscoelasticity of a fluid at a particular mechanical resonance frequency which is determined by the dimensions of the apparatus [Fritz *et al.* (2003)]. A schematic of the TR is shown in Fig. 2(a). The TR consists of a cylindrical vessel of radius 10 mm and total length 60 mm and a central torsion tube fitted with piezos and a temperature sensor. Four PZTs are embedded within the central tube, as shown in Fig. 2(a). Two active PZTs provide a torsional motion of the TR and two passive PZTs are used to detect the sample response. The test fluid is introduced between the outer cylinder and the central torsion tube. The TR is then hermetically closed. Figure 2(b) shows a photograph of the outer cylinder and inner tube. In the present work, the TR has been used at a temperature of 25 ± 0.1 °C with temperature stability during individual experiments of 0.01 °C. In a similar way to the PAV, the TR is operated by a lock-in-amplifier (SR 850, Stanford Research Systems) with exciting voltages between 0.2 and 1 V, depending on the fluid viscosity, resulting in a torsion of amplitude of about 100 nm,

$$\begin{aligned} \mathrm{Re}(\upsilon) &= \mathrm{A}(\upsilon) \cdot \cos(\varphi), \\ \mathrm{Im}(\upsilon) &= \mathrm{A}(\upsilon) \cdot \sin(\varphi). \end{aligned} \tag{3}$$

The TR was excited at frequencies in the vicinity of the resonance frequency, i.e., about 25 500 and 77 500 Hz in the present work, and the voltage amplitude $\mathrm{A}(\upsilon)$ and the absolute value of the phase $\varphi(\upsilon)$ were measured by the lock-in-amplifier. The frequency response was split into real and imaginary parts [see Eq. (3)] which are subsequently approximated by a model for mechanical resonators [Eq. (4)]

$$\mathrm{Re}(\upsilon) = \mathrm{A}_0 \mathrm{f} \frac{\mathrm{D}^2 \upsilon}{(\mathrm{f}^2 - \upsilon^2)^2 + \mathrm{D}^2 \upsilon^2},$$

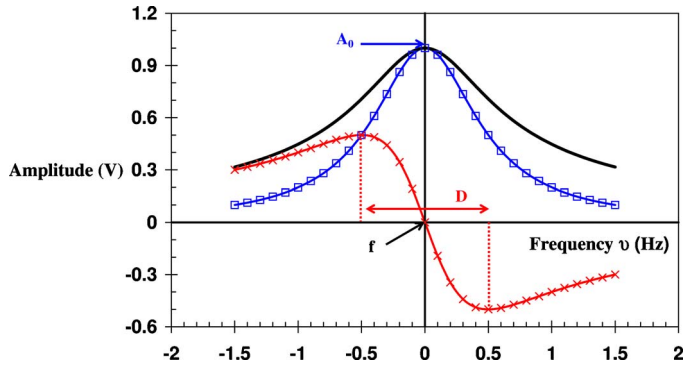

FIG. 3. Amplitude A(υ) of the signal measured from the TR from which A, f, and D are extracted. (−) Solid line represents the measured signal (loaded or unloaded), (–□–) the real, and (–×–) the imaginary parts approximated by the theoretical resonance expression [Eq. (4)]. Figure reproduced from Fritz *et al.* (2003).

$$\mathrm{Im}(\upsilon) = A_0 f \frac{D(f^2 - \upsilon^2)}{(f^2 - \upsilon^2)^2 + D^2\upsilon^2}, \tag{4}$$

where f is the resonance frequency, D is the damping of the oscillation, and A_0 is the constant amplitude of the signal (Fig. 3). The calibration f_{air} and D_{air} values are extracted from the resonance frequency signal of the resonator when unloaded. The immersion of the resonator within the test sample results in a lower and broader resonance frequency signal from which f_{sample} and D_{sample} are extracted. The changes in resonance frequency Δf and damping of the oscillation ΔD are calculated as follows:

$$\begin{aligned} \Delta D &= D_{sample} - D_{air}, \\ \Delta f &= f_{sample} - f_{air}, \end{aligned} \tag{5}$$

which are subsequently introduced into Eq. (6) to determine the elastic modulus G′ and the loss modulus G″ [Fritz *et al.* (2003]

$$\begin{aligned} G' &= \frac{k}{\rho}\left[\left(\frac{\Delta D}{2}\right)^2 - \Delta f^2\right], \\ G'' &= -\frac{1}{\rho}\Delta D \Delta f, \end{aligned} \tag{6}$$

where ρ is the sample density and k is the instrument constant. More details of the TR calculation process can be found in Fritz *et al.* (2003).

C. Fluid characteristics

Three series of samples were investigated and their physical properties are reported in Table I. The first series I was a low viscosity polymeric solution based on a monodisperse polystyrene with a molecular weight of 110 kg/mol (PS110) at different weight concentrations (0, 0.1, 0.2, 0.5, 1, 2.5, and 5 wt %) dissolved in diethyl phthalate (DEP). In addition within this series, a sample of 10 wt % of PS210 dissolved in DEP was used to match mechanical spectrum data and data obtained from PAV experiments.

The series II and III fluids were made from a ultraviolet (UV) ink jet fluid provided SunJet, the ink jet division of SunChemical®. These two series were prepared using a

TABLE I. Fluid properties.

	Series I	Series II	Series III
Solvent	Diethyl phtalate	Poly-acrylate	Poly-acrylate
Viscoelastic enhancer	Polystyrene (110 kg/mol)	Phthalocyanine blue organic particle and acrylate monomer (10–20 kg/mol)	Phthalocyanine blue organic particle and acrylate monomer (10–20 kg/mol)
c^*	2.67 wt %		
Key variables	0–5 wt %	0–10 wt %	0–8 wt %
η_0 at 25 °C	10–68 mPa s	32–122 mPa s	29.3–33 mPa s
σ	37 mN/m	32 mN/m	32 mN/m
ρ	1120 kg/m^3	1050 kg/m^3	1050 kg/m^3

pigment paste containing 25 wt % of phthalocyanine blue organic particles (average diameter ~100 nm) dispersed in 44 wt % low molecular polydisperse acrylate-monomers (molecular weight of 16 kg/mol) and diluted in a Newtonian poly-acrylate UV varnish with a base viscosity of 20 mPa s. Series II considers different particle weight concentrations of phthalocyanine blue organic particles (0, 2, 4, 6, 8, and 10 wt %) and subsequently low molecular weight polymer, diluted in a Newtonian poly-acrylate UV varnish with a base viscosity of 20 mPa s. Series III is a base viscosity matched series of fluids consisting of different particle weight concentrations of phthalocyanine blue organic particles (0, 2, 4, 6, and 8 wt %) diluted in a mixture of Newtonian poly-acrylate UV varnishes of base viscosities 10, 20, and 30 mPa s in order to obtain a final fixed base viscosity for each fluid of 32 mPa s at 25 °C. For series II and III samples, the particle weight concentration will be specified.

Finally, an industrial drop on demand magenta ink (particle size about 100 nm) of base viscosity 33 mPa s at 25 °C, manufactured by SunJet®, was used to provide comparison data for a commercial ink jet fluid.

III. EXPERIMENTAL RESULTS

The PAV was validated against a parallel plate oscillatory rheometer (ARES, TA Instruments) using the 10 wt % PS210 diluted in DEP fluid and data for this fluid are shown in Fig. 4. The viscosity of the fluid is sufficiently high that parallel plate oscillatory rheometer data can be obtained in the frequency range of 0.1–16 Hz. An overlapping set of PAV data for the same fluid was obtained from 3 to 10 000 Hz. This figure shows that there is a reasonable match between the parallel plate oscillator rheometer and the PAV data in the overlapping region. The low frequency limit of a single mode Maxwell fluid should give a limiting slope of one for the $G''(\omega)$ data curve and a slope of two for $G'(\omega)$ data. The parallel plate oscillator rheometer data presented in Fig. 4 give a low frequency ($f < 1$ Hz) G'' slope of 1; however, the G' data slope is less than 2 and the fluctuations in the curve suggests that, in this region, the data are subject to experimental noise.

Figure 5 shows the LVE data for both the PAV and TR for a 2.5 wt % series I test fluid. The PAV data were obtained between 30 and 10 000 Hz and the TR data at the two TR resonant frequencies close to 25 500 and 77 500 Hz. Overlapping data are not possible using these two rheometers; however, from the results shown in Fig. 5, consistency between the two data sets appears reasonable.

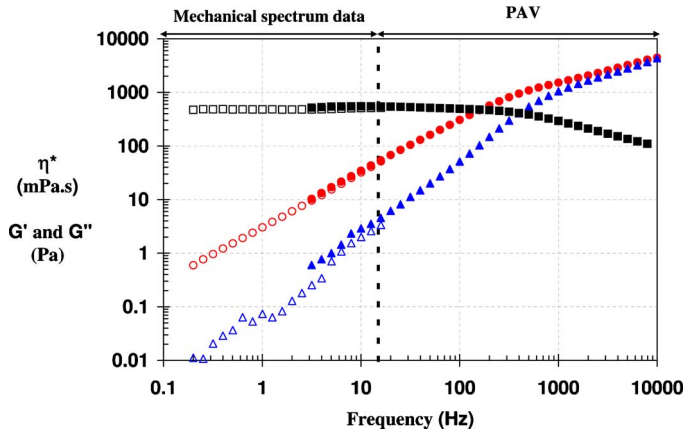

FIG. 4. Matching mechanical spectrum data (ARES, empty symbols) and PAV data (full symbols). Fluid: DEP-10 wt % of monodisperse polystyrene 210 kg/mol. (■) η^*, (●) G″, and (▲) G′.

For both the polymer fluids tested, the low frequency slope of the G″ curve is close to 1 and the G′ curve close to 2. This is consistent with the characteristic of a "Maxwell fluid" following the classical form of the single mode Maxwell equations given below [see, for example, Han (1976)]

$$\mathrm{G}'' = \eta_s\omega + \frac{\mathrm{g}\omega\tau}{1+(\omega\tau)^2} \approx \omega(\eta_s + \mathrm{g}\tau),$$

$$\mathrm{G}' = \frac{\mathrm{g}(\omega\tau)^2}{1+(\omega\tau)^2} \approx \mathrm{g}(\omega\tau)^2, \tag{7}$$

$$\eta^* = \frac{\sqrt{\mathrm{G}'^2 + \mathrm{G}''^2}}{\omega},$$

where η_s is the solvent viscosity, g is the elastic modulus of the Maxwell element, and τ is the relaxation time of the Maxwell element. The data presented in Figs. 4 and 5

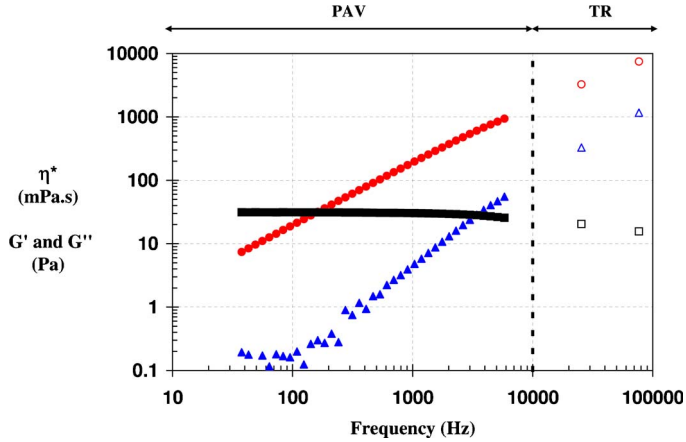

FIG. 5. Matching PAV data (full symbols) and TR data (empty symbol). Fluid: DEP-2.5 wt % of monodisperse polystyrene 110 kg/mol. (■) η^*, (●) G″, and (▲) G′.

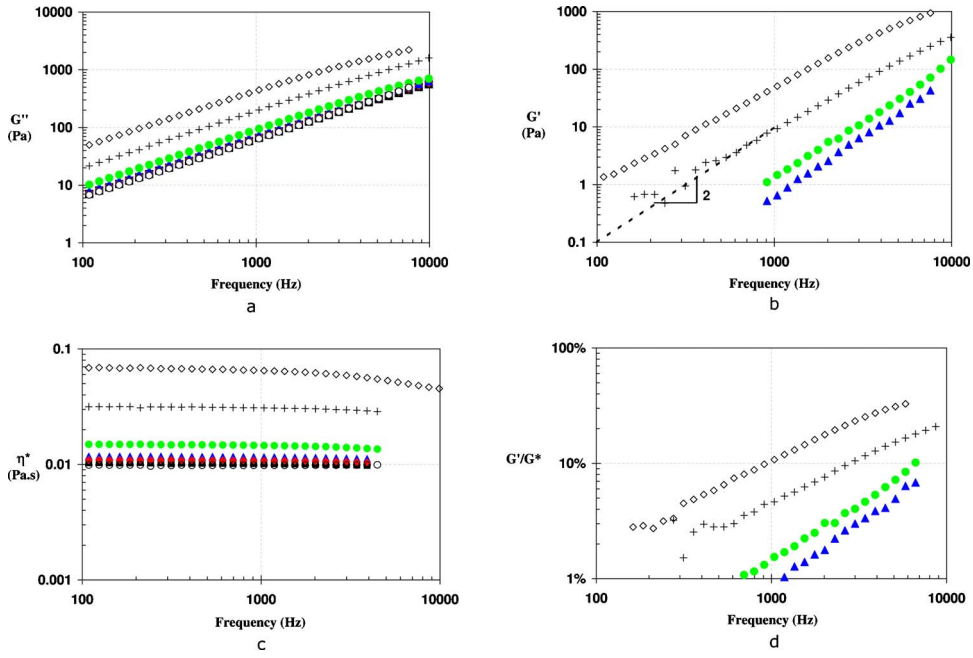

FIG. 6. Series I fluids. (a) Loss modulus G″, (b) elastic modulus G′, (c) complex viscosity η^* and (d) elastic ratio of solution of DEP-PS 110 000 at different concentrations. (○) DEP, (■) DEP-0.1%PS, (♦) DEP-0.2%PS, (▲) DEP-0.4%PS, (●) DEP-1%PS, (+) DEP-2.5%PS, and (◇) DEP-5%PS. Dashed line on G′ graph represents a power law of index 2.

indicate that the parallel plate oscillatory rheometer, the PAV, and the TR appear to give self-consistent results for the respective frequency regimes that they can explore.

A. Series I fluids: The effect of polymer additive

The effect of polymer loading on the low viscosity LVE for a polymer solution is shown for series I fluids in Fig. 6. G″ develops in the anticipated way, as shown in Fig. 6(a), with a linear slope as a function of frequency and a vertical shift with increasing concentration of polymer. The development of G′ with polymer loading is shown in Fig. 6(b). The pure DEP solution, which is a low molecular weight molecule, does not show a G′ response on the range of frequencies investigated confirming its Newtonian behavior. As polymer loading increases, the G′ response increases and extends to progressively lower frequencies. The slopes of the G′ curves tend to follow a gradient of 2 in a consistent manner predicted by a simple Maxwell fluid and the relaxation time that can be extracted from these data are comparable to the drive pulse width. The evolution of the complex viscosity η^* is shown in Fig. 6(c) and here it can be seen that the fluids, while being viscoelastic, are essentially Newtonian in that their complex viscosities at all concentrations are essentially independent of frequency. However, the mainly Newtonian behavior of the fluid does not prevent the viscoelasticity of the fluid playing an important role on the ink jetting velocity, filament break-up, and satellite formation [Xu *et al.* (2007); Vadillo *et al.* (2010)]. In terms of ink jet printing, it has recently been established that the ratio of G'/G^*, shown in Fig. 6(d), is an important quantity [Hoath *et al.* (2009)] that enables the determination of the jetting quality of the fluid.

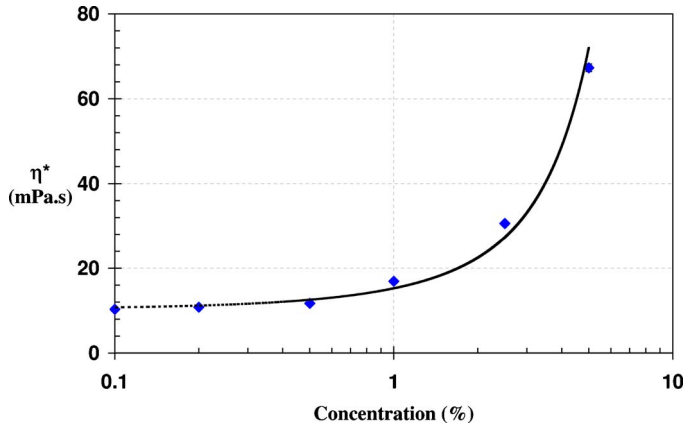

FIG. 7. Complex viscosity enhancement for series I polymer additive fluids.

The complex viscosity of the series I polymer solutions is plotted in Fig. 7 as a function of polymer concentration and as expected after an initial linear slope, the viscosity increases in a nonlinear fashion above a critical concentration of about 1% for this particular molecular weight polymer [Thomas and Thomas (1960)]. The overall response of the polymer solutions is consistent with that of a Maxwell fluid where the origin of elasticity originates from the entropic elasticity of the coiled polymer chains.

B. Series II and III fluids: The effect of particle loading

The rheological measurements performed on the series II particle laden samples are shown in Fig. 8 in a similar way to the series I polymer solution of Fig. 6. Again, the G″ response shown in Fig. 8(a) is as expected with a slope of 1 and there is a vertical shift with increasing particle loading. The G′ data shown in Fig. 8(b) indicate a strong development with particle concentration; however, the gradients of the curves in this case are now closer to 1 rather than 2 as seen for the polymer solution. The base varnish does not exhibit a G′ response over the frequency range of investigation which confirms its Newtonian behavior. The plot of complex viscosity as a function of frequency shown in Fig. 8(c) again demonstrates that this fluid is essentially Newtonian up to 6 wt % concentration while at the same time being viscoelastic. With increasing concentration (8%–10%), the fluid shows non-Newtonian "shear thinning" behavior. The development of G′ is striking and when plotted as the ratio of G'/G^* shows a strong effect at all frequencies plotted [Fig. 8(d)].

Figure 9 shows the way η^* develops with particle concentration and again a similar trend to the polymer solution case shown in Fig. 7 is seen. The base viscosity starts to rise significantly above a concentration of about 1 wt % of particles.

In order to assess the response for particle loading alone without changing the base viscosity, series III fluids were formulated using solvents with different viscosities. Results are presented for both PAV and TR measurements in Fig. 10. The G″ and η^* developments shown in Figs. 10(a) and 10(c), respectively, show that base viscosity matching has been achieved. Figure 10(b) shows the development of G′ and demonstrates that this effect is essentially independent of the base viscosity of each fluid as this is the same. The TR results appear to follow a reasonable extrapolation of the PAV results although the TR results do suggest a small amount of high frequency shear thinning of the fluids.

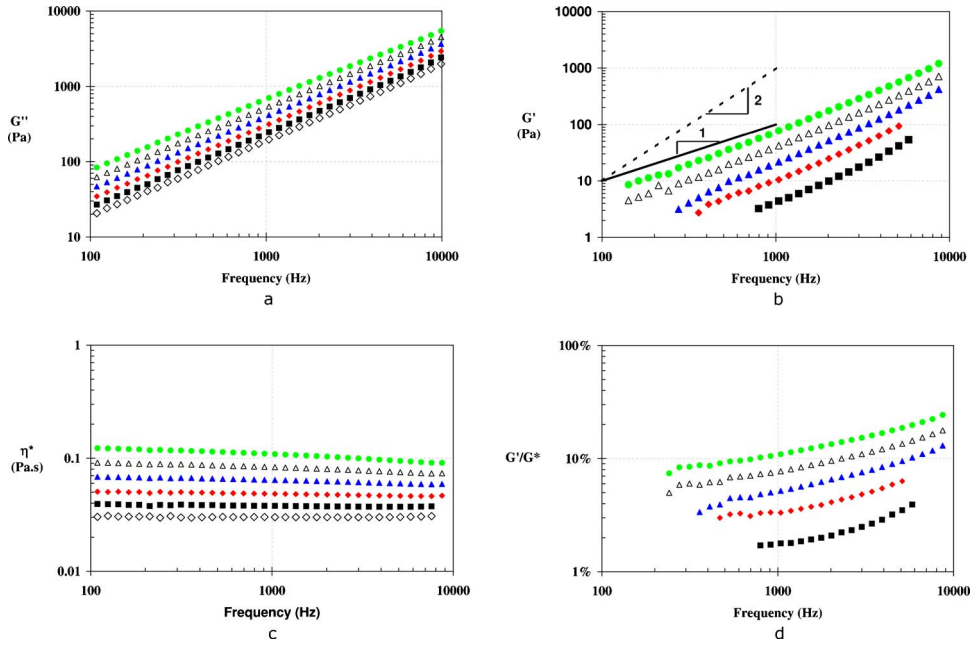

FIG. 8. Series II fluids. (a) Loss modulus G″, (b) elastic modulus G′, (c) complex viscosity η^*, and (d) elastic ratio of solution of UV varnish 1 and pigment paste at different weight concentrations. (◇) Varnish, (■) varnish-2 wt % pigment, (◆) varnish-4 wt % pigment, (▲) varnish-6 wt % pigment, (△) varnish-8 wt % pigment, and (●) varnish-10 wt % pigment.

The observation of a G′ development with particle addition has been reported before [see, for example, Lobe and White (1979); Leonov (1990); Tsenoglou and Yang (1990); Aoki *et al.* (2003a, 2003b); Aoki and Watanabe (2004); Aoki (2007); Zmievski *et al.* (2007)] where slopes of G′ closer to 1 than 2 have been seen. A particular index of 1.2 has been measured for all samples of series II and this contrasts with the polymer solution case of a slope of 2. While it is possible to construct G′ slopes of 1 using a multimode Maxwell model [see, for example, Mackley *et al.* (1994)], it seems more likely that the

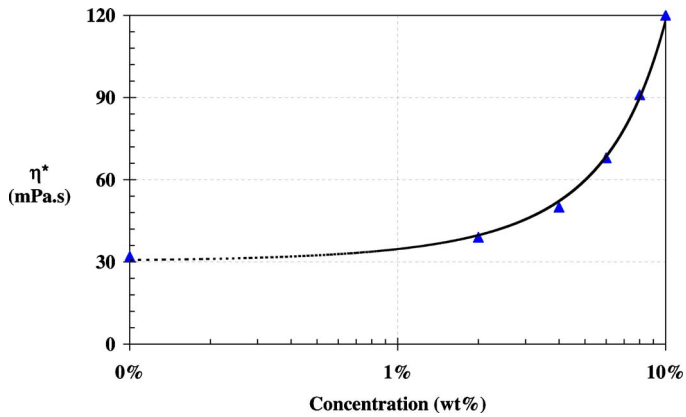

FIG. 9. Complex viscosity enhancement for series II particle additive fluids.

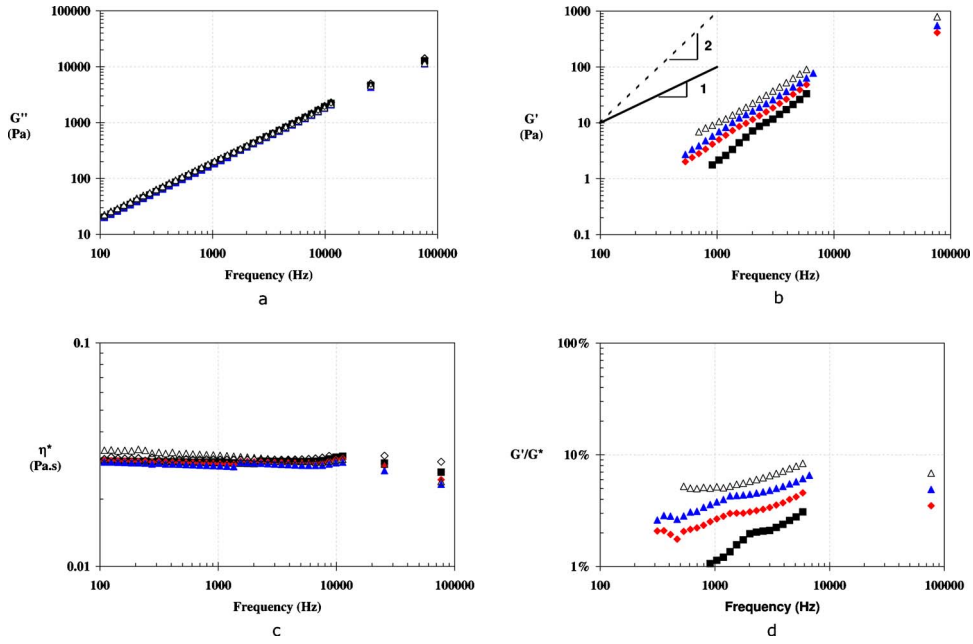

FIG. 10. Series III fluids. (a) Loss modulus G″, (b) elastic modulus G′, (c) complex viscosity η^*, and (d) elastic ratio of solution of mixture of UV varnishes and pigment paste at different weight concentrations. (◇) Varnish, (■) varnishes mixture-2 wt % pigment, (♦) varnishes mixture-4 wt % pigment, (▲) varnishes mixture-6 wt % pigment, and (△) varnishes mixture-8 wt % pigment.

mechanism of G′ development is different for particles when compared with polymers. Clearly inter-particle interactions are anticipated and presumably this gives rise to the observed G′ development.

C. Commercial ink jet fluid

The LVE response of a commercial printing ink is shown in Fig. 11 for both PAV and

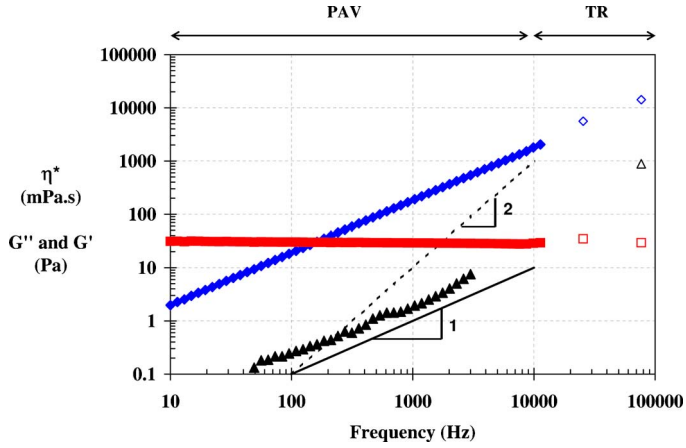

FIG. 11. High frequency LVE data of a commercial UV ink jet printing ink measured at 25 °C with (a) the PAV (full symbols) and (b) the TR (empty symbols). (■, □) η^*, (♦, ◇) G″, and (▲, △) G′.

TR data. The results show a similar trend to the model inks in that the complex viscosity over the whole test frequency range remains constant and the G″ slope is 1. The G′ slope falls between 1 and 2 in the region of 1.2. This result is consistent with previous work of Potanin *et al.* (1995) who considered the case of weakly aggregated polystyrene latex dispersions where G′ was predicted theoretically and demonstrated experimentally to increase with the volume fraction at high frequency. The fact that ink jet fluids can be viscoelastic has been reported [Hoath *et al.* (2009); Vadillo *et al.* (2010)] and they have shown that this elasticity can effect ink jet printing performance. Both base viscosity and elasticity effects influence the way ink jet fluids leave the ink nozzle and also subsequently break up after leaving the nozzle. It is clear from data of the type shown in Fig. 11 that in order to access the frequency domain where G′ is present, both PAV and TR rheometers are necessary. The G′ slope of 1.2 suggests that particle interaction rather than polymer elasticity is the most dominant elastic mode for the commercial ink jet fluid, although interpretation of microstructural behavior from LVE data should be carried out with caution.

IV. DISCUSSION AND CONCLUSIONS

This paper has demonstrated that by using a PAV and a TR, it is possible to characterize LVE for low viscosity fluids containing both polymer and particles. The addition of polymer to a low viscosity matrix has the anticipated effect of overall complex viscosity enhancement. In addition, over the frequency range tested, the viscosity did not exhibit shear thinning with η^* essentially independent of the frequency. Again, as anticipated, the introduction of polymer resulted in the progressive development of the elasticity resulting in a "Maxwell-like" behavior with a G′ slope of order of 2 and a G″ slope of order of 1. The data can be used to extract a single mode Maxwell relaxation time for each sample tested.

As with the polymer, the addition of particle results in the development of the complex viscosity with the particle loading. A development of a high frequency elasticity was also observed; however, in this case the response was not Maxwellian and the G′ slope was found to be closer to 1 than 2. The observed noninteger behavior of the slope of G′ was assumed to come from the complex nature of the fluid particle-particle interaction.

Commercial ink jet formulation can be characterized using the PAV and the TR and this work has presented data for a series of model ink jet fluids where the base complex viscosity has been matched with different particle loading. The results show that the evolution of G′ depends on the particle loading regardless of any base viscosity change.

From the results presented here and in combination with previous reported work, it can be concluded that G′ and G″ data can be obtained over a frequency range between 0.1 and 77 000 Hz for low viscosity fluids. This point is particularly useful because, unlike high viscosity melts where temperature/frequency superposition can extend the frequency ranges, this in general is not possible for ink jet or biological fluids.

ACKNOWLEDGMENTS

D.V. would like to thank the Industry/EPSRC funded Ink Jet Centre of Excellence for financial support and A.M. would like to thank Xaar PLC for providing Ph.D. funding. The authors would also like to acknowledge Professor Pechhold and his team at the University of Ulm for their assistance with both the PAV and TR rheometers.

References

Aoki, Y., "Rheological characterization of carbon black/varnish suspensions," Colloids Surf., A **308**, 79–86 (2007).

Aoki, Y., A. Hatano, and H. Watanabe, "Rheology of carbon black suspensions. I. Three types of viscoelastic behavior," Rheol. Acta **42**, 209–216 (2003a).

Aoki, Y., A. Hatano, and H. Watanabe, "Rheology of carbon black suspensions. II. Well dispersed system," Rheol. Acta **42**, 321–325 (2003b).

Aoki, Y., and H. Watanabe, "Rheology of carbon black suspensions. III. Sol-gel transition system," Rheol. Acta **43**, 390–395 (2004).

Auhl, D., J. Ramirez, A. E. Likhtman, P. Chambon, and C. Fernyhough, "Linear and nonlinear shear flow behavior of monodisperse polyisoprene melts with a large range of molecular weights," J. Rheol. **52**, 801–835 (2008).

Basilevsky, A. V., J. D. Meyer, and A. N. Rozhkov, "Dynamics and breakup of pulse microjets of polymeric liquids," Fluid Dyn. **40**(3), 376–392 (2005).

Bergenholtz, J., N. Willenbacher, N. J. Wagner, B. Morrison, D. van den Ende, and J. Mellema, "Colloidal charge determination in concentrated liquid dispersions using torsional resonance oscillation," J. Colloid Interface Sci. **202**, 430–440 (1998).

Crassous, J., R. Régisser, M. Ballauff, and N. Willenbacher, "Characterization of the viscoelastic behavior of complex fluids using the piezoelastic axial vibrator," J. Rheol. **49**, 851–863 (2005).

Dong, H., W. W. Carr, and J. F. Morris, "An experimental study of drop-on-demand drop formation," Phys. Fluids **18**, 072102 (2006).

Ferry, J. D., *Viscoelastic Properties of Polymers* (Wiley, New York, 1980).

Fritz, G., W. Pechhold, N. Willenbacher, and N. J. Wagner, "Characterizing complex fluids with high frequency rheology using torsional resonators at multiple frequencies," J. Rheol. **47**(2), 303–319 (2003).

Fromm, J. E., "Numerical calculation of the fluid dynamics of drop-on-demand jets," IBM J. Res. Dev. **28**, 322–333 (1984).

Groß, T., L. Kirschenmann, and W. Pechhold, "Piezo axial vibrator (PAV)—A new oscillating squeeze flow rheometer," *Proceedings of the Eurheo*, Erlangen, 2002 (European Society of Rheology).

Han, C. D., *Rheology in Polymer Processing* (Academic, London, 1976).

Hoath, S. D., I. M. Hutchings, G. D. Martin, T. R. Tuladhar, M. R. Mackley, and D. C. Vadillo, "Link between ink rheology, drop-on-demand jet formation and printability," J. Imaging Sci. Technol. **53**(4), 041208 (2009).

Jang, D., D. Kim, and J. Moon, "Influence of fluid properties on ink-jet printability," Langmuir **25**, 2629–2635 (2009).

Kirschenmann, L., Ph.D. thesis, University of Ulm, 2003.

Kirschenmann, L., and W. Pechhold, "Piezoelectric rotary vibrator (PRV)—A new oscillating rheometer for linear viscoelasticity," Rheol. Acta **41**, 362–368 (2002).

Leonov, A. I., "On the rheology of filled polymers," J. Rheol. **34**(7), 1039–1067 (1990).

Lobe, V. M., and J. L. White, "An experimental study of the influence of carbon black on the rheological properties of a polystyrene melt," Polym. Eng. Sci. **19**(9), 617–624 (1979).

Mackley, M. R., R. T. J. Marshall, J. B. A. F. Smeulders, and F. D. Zhao, "The rheological characterization of polymeric and colloidal fluids," Chem. Eng. Sci. **49**(16), 2551–2565 (1994).

Macosko, C. W., *Rheology—Principles, Measurements and Applications* (Wiley-VCH, 1994).

Potanin, A. A., R. De Rooij, D. Van den Ende, and J. Mellema, "Microrheological modeling of weakly aggregated dispersions," J. Chem. Phys. **102**(14), 5845–5853 (1995).

Theobald, S., P. Schwarzenberger, and W. Pechhold, "Measurements of the complex shear modulus of polymers under hydrostatic pressure using the quartz resonator method," High Press. Res. **13**(1), 133–140 (1994).

Thomas, D. K., and T. A. J. Thomas, "Viscosity-concentration relationships in solutions of high polymers," J. Appl. Polym. Sci. **3**, 129–131 (1960).

Tsenoglou, C., and S. Yang, "Fluidity and optimum packing in suspensions of mixed dissimilar particles," Polym. Eng. Sci. **30**, 1407–1412 (1990).

Tuladhar, T. R., and M. R. Mackley, "Filament stretching rheometry and break-up behaviour of low viscosity polymer solutions and ink jets fluids," J. Non-Newtonian Fluid Mech. **148**, 97–108 (2008).

Vadillo, D. C., T. R. Tuladhar, A. C. Mulji, M. R. Mackley, S. Jung, and S. D. Hoath, "The development of the 'Cambridge Trimaster' filament stretch and break-up device for the evaluation of ink jet fluids," J. Rheol. **54**(2), 261–282 (2010).

Walters, K., "Something old, something new, in rheometry," J. Central South Uni. Tech. **14**, 10–13 (2007).

Whorlow, R. W., *Rheological Techniques*, 2nd ed. (Ellis Horwood, New York, 1992).

Willenbacher, N., C. Oelschlaeger, and M. Schopferer, "Broad bandwidth optical and mechanical theometry of wormlike micelle solutions," Phys. Rev. Lett. **99**, 068302 (2007).

Xu, D., V. Sanchez-Romaguera, S. Barbosa, W. Travis, J. De Wit, P. Swan, and S. G. Yeates, "Inkjet printing of polymer solutions and the role of chain entanglement," J. Mater. Chem. **17**, 4902–4907 (2007).

Zmievski, V., M. Grmela, and M. Bousmina, "Suspensions of rigid spherical particles in polymeric solutions," Physica A **376**, 51–74 (2007).